CrystEngComm

PAPER

View Article Online
View Journal | View Issue

Cite this: *CrystEngComm*, 2022, **24**, 3049

A pre-reaction suppressing strategy for α-Ga_2O_3 halide vapor pressure epitaxy using asymmetric precursor gas flow†

Sunjae Kim,‡[abf] Hyeon Woo Kim,‡[cd] Hyeong-Yun Kim,[ae] Dae-Woo Jeon,[a] Sung Beom Cho *[c] and Ji-Hyeon Park *[a]

Received 16th February 2022,
Accepted 7th March 2022

DOI: 10.1039/d2ce00222a

rsc.li/crystengcomm

We report on a high-quality α-Ga_2O_3 epilayer grown on a sapphire (0001) substrate by suppressing the pre-reaction between the main precursors, GaCl and $GaCl_3$, and O_2. The carrier gas flow rate and susceptor position had the greatest influence as key factors for the crystal quality of the α-Ga_2O_3 epilayer and the thickness uniformity in the sapphire (0001) substrate. By increasing the carrier flow rate of the inner tube to which GaCl and $GaCl_3$ are supplied, the phenomenon of pre-reacting with an O_2 precursor before reaching the substrate was suppressed. Furthermore, a suitable growth position of the susceptor allowed for a uniform distribution of the growth temperature and main precursors, thereby resulting in the growth of a high-quality and uniform α-Ga_2O_3 epilayer on the substrate. Multiscale-multiphysics simulation on reactors soundly supports the relationship between the growth quality and process conditions such as the velocity of the gases, susceptor position, and temperature. Our results suggest that the carrier gas flow rate, susceptor position, and temperature should be carefully controlled for growing high-quality epilayers.

Introduction

There has been a recent surge of interest in the ultra-wide bandgap power semiconductor gallium oxide (Ga_2O_3).[1–3] In particular, Ga_2O_3 has five polymorphs (α, β, ε, δ, and γ) with various band gaps, ranging from 4.8 eV to 5.3 eV, depending on the phase.[4,5] Among the various phases, α- and β-Ga_2O_3 are the most commonly studied for power semiconductor devices.[6–9] This is because the β-phase is very stable at high temperatures; therefore, it offers the advantage of enabling mass-production of bulk wafers and homoepitaxial growth.[10] In the case of α-Ga_2O_3, it is not possible to manufacture a homo substrate because it exhibits a stable phase at low temperatures of 500 °C or less; however, it has an advantage in high-quality heteroepitaxial growth with a sapphire substrate, which has a relatively small lattice mismatch (*a*-axis: 4.5%, *c*-axis: 3.3%) compared with GaN and sapphire.[11] Furthermore, α-Ga_2O_3 has the widest bandgap of 5.3 eV among Ga_2O_3 phases;[12] therefore, a very high breakdown field is predicted, which will be useful in high-performance power semiconductor applications with better figures of merit.[13]

Consequently, many researchers have proposed various methods, such as molecular beam epitaxy (MBE),[14] mist-chemical vapor deposition (CVD),[15] and halide vapor phase epitaxy (HVPE),[16] to grow high-quality α-Ga_2O_3 epilayers. As is well known, MBE provides excellent performance in growing high-quality α-Ga_2O_3 epilayers; however, the growth rate is extremely low. Thus, most recent research is focused on mist-CVD and HVPE methods with mass-productivity and scalability. Mist-CVD is a method for growing an α-Ga_2O_3 epilayer using droplets of a mist form using ultrasound, and HVPE is a method for growing an α-Ga_2O_3 epilayer by converting liquid Ga into GaCl and $GaCl_3$ using HCl. Although both methods are known to result in the growth of high-quality α-Ga_2O_3 epilayers, the HVPE method has the advantage of several times faster growth rate compared to mist-CVD.[13] For this reason, the HVPE method is mainly used in research to rapidly grow high-quality α-Ga_2O_3 epilayers.

Intensive studies on growing α-Ga_2O_3 epilayers using HVPE have been conducted, and various parameters, such as the VI/III ratio control, pre-treatment process, growth mode, temperature, and others, have been utilized to enhance the

[a] *Korea Institute of Ceramic Engineering and Technology, Jinju, Gyeongsangnam-do 52851, Republic of Korea. E-mail: jhp5511@kicet.re.kr*
[b] *Department of Materials Science and Engineering, Korea Aerospace University, Goyang, 10540, Republic of Korea*
[c] *Convergence Technology Division, Korea Institute of Ceramic Engineering and Technology (KICET), Jinju-si 52851, Republic of Korea. E-mail: csb@kicet.re.kr*
[d] *Division of Materials Science and Engineering, Hanyang University, Seoul, 04763, Republic of Korea*
[e] *Department of Material Science and Engineering, Pukyong National University, Busan, 48513, Republic of Korea*
[f] *Department of Smart Air Mobility, Korea Aerospace University, Goyang, 10540, Republic of Korea*

† Electronic supplementary information (ESI) available. See DOI: **https://doi.org/10.1039/d2ce00222a**

‡ These authors equally contributed to this work.

growth quality.[17–21] One of the most crucial criteria for film quality is related to the pre-reaction. Because the precursor gas in HVPE is highly reactive, the α-Ga_2O_3 epilayer can be formed before reaching the substrate.[22] This pre-reaction leads to the formation of powder that can cause serious contamination of the whole reactor and deterioration of the epilayer quality. The adhesion of this powder on substrates introduces large defects that can significantly degrade the device performance. To avoid the pre-reaction, the process parameters should be intensively utilized. However, the process requires numerous trials and errors owing to the difficulty of observation of the inside of the chamber. To solve these issues, virtually simulated modeling of the HVPE system can be used, which can provide useful information on the inside of the chamber by providing further insights into gas flow dynamics and growth conditions.[23,24] With the combination of experimental growth characterization and surrogate modeling, development of a strategy for avoiding the pre-reaction of α-Ga_2O_3 is highly desired.

In this study, we utilized both experiments and simulations to unveil the physics inside a HVPE chamber, and suggested a strategy to suppress the pre-reaction through utilization of carrier gas supply. We identified the thermodynamics of the pre-reaction chemistry using density-functional-theory (DFT)-based energetics, and constructed multiphysics finite-element method (FEM) models to analyze fluid dynamics and heat transfer inside the chamber. Using the simulation models, we performed parametric studies on gas flow rates, temperature, and susceptor positions. The experimental growth and characterization were also performed simultaneously for direct comparison. The correlation between gas flow dynamics and growth quality was investigated by analyzing high-resolution X-ray diffraction system (HR-XRD) and X-ray photoelectron spectroscopy (XPS) characterization data with the corresponding simulation data. Thorough screening of various parameters revealed that the asymmetric carrier gas flow between the inner tube and the outer-shell effectively suppressed the pre-reaction. Furthermore, the susceptor position also plays a complementary role in optimizing the growth conditions.

Experimental

α-Ga_2O_3 growth using HVPE equipment

Fig. 1 shows a schematic illustration of the HVPE reactor structure and gas lines. The main precursors GaCl and $GaCl_3$ were formed by the reaction of liquid gallium (99.9999%) with HCl (99.999%). GaCl and $GaCl_3$ were supplied through the inner tube, O_2 (99.999%) was supplied from the outer-shell, and N_2 (99.999%) was used as the carrier gas. Using HVPE equipment, α-Ga_2O_3 epilayers were grown on a 2 inch sapphire (0001) substrate with different inner tube carrier gas flow rates and susceptor positions. The 2 inch sapphire substrate was cleaned through an HCl cleaning process in HVPE. The asymmetric carrier gas represents different amounts of carrier gas supplied to the inner tube and outer-shell of the HVPE reactor. The inner tube carrier gas flow rate was adjusted from 1100 sccm to 3900 sccm, and the total flow rate of the gas supplied to the outer-shell was 600 sccm. The susceptor position was adjusted from 5 cm to 11 cm as the distance from the edge of the inner tube to the substrate. All other experimental conditions were fixed. The HVPE reactor is divided into a source region and a growth region, and the horizontal wall contains a resistance heater to maintain the growth temperature. The temperature of the source and growth regions was fixed at 470 °C. The growth of Ga_2O_3 was according to the equation:[25]

$$2GaCl(gas) + 3/2O_2(gas) \rightarrow Ga_2O_3(solid) + Cl_2(gas) \quad (1)$$

$$2GaCl_3(gas) + 3/2O_2(gas) \rightarrow Ga_2O_3(solid) + 3Cl_2(gas) \quad (2)$$

Material characterization

The surface morphology was examined by optical microscopy (OM, Olympus, Tokyo, Japan) and the cross-view was analyzed using scanning electron microscopy (SEM, EM-30, COXEM). Surface roughness characteristics were evaluated through atomic force microscopy (AFM, DAIL SYSTEMS, Korea). The growth thickness was measured using an F20-UV analyzer (KLA Corporation, USA). To analyze the structure and crystal quality of the epilayer, 2θ, rocking curve, and phi

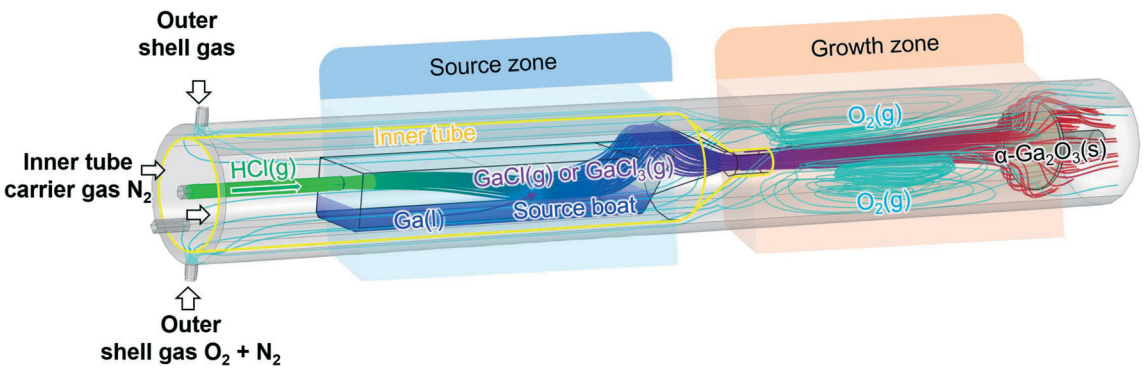

Fig. 1 Schematic illustration of the structure of an HVPE reactor and gas lines for α-Ga_2O_3 growth.

scans were performed using HR-XRD (Rigaku SmartLAB, Tokyo, Japan) with Cu Kα_1 radiation (λ = 0.15405 nm) and XPS (Thermo Fisher Scientific, K-ALPHA+ System).

Density functional theory calculations

DFT calculations were performed using the Vienna *ab initio* simulation package (VASP).[26] The projector-augmented wave potential was applied with the generalized gradient approximation within the Perdew–Burke–Ernzerhof framework.[27] The 3d, 4s, and 4p states of Ga, 3s and 3p states of Cl, and 2s and 2p states of O were considered as the valence states. Input parameters were set as follows: energy cutoff = 520 eV, energy criteria = 10^{-5} eV, and force criteria = 0.05 eV Å^{-1}. The *k*-point sampling for bulk relaxation was used for the Monkhorst–Pack[28] method with a 6 × 6 × 2 grid. Energy calculations of the molecule were performed with a cubic unit cell (10 Å × 10 Å × 10 Å) and Γ-point only sampling in reciprocal space.

The thermodynamic energetics calculation was based on DFT-driven Gibbs free energy. The Gibbs free energies for the formation of α-Ga_2O_3 through the reaction paths (1) and (2) are calculated as follows:

$$\Delta G_{\mathrm{rxn1}} = \mu_{\mathrm{Ga_2O3}} + \mu_{\mathrm{Cl_2}} - 2\mu_{\mathrm{GaCl}} - 3\mu_{\mathrm{O}} \quad (3)$$

$$\Delta G_{\mathrm{rxn2}} = \mu_{\mathrm{Ga_2O3}} + 3\mu_{\mathrm{Cl_2}} - 2\mu_{\mathrm{GaCl_3}} - 3\mu_{\mathrm{O}} \quad (4)$$

where μ represents the chemical potential of each reactant or product. Based on the ideal gas assumption, the chemical potential depends on the reaction temperature and partial pressure as follows:

$$\Delta\mu_i(T,p) = \mu_i^0 + k_{\mathrm{B}}T\ln\left(\frac{p_i}{p_i^0}\right) \quad (5)$$

where μ_i^0 is the internal energy of i that was extracted from the DFT calculation, k_{B} is the Boltzmann constant, T is temperature, p is pressure, and p^0 is the pressure in the standard state. In eqn (5), the former term represents the internal energy under standard conditions, and the latter term represents the activity term. The activity term of solid-state α-Ga_2O_3 is set to zero because the pressure dependency of the activity in the solid phase is negligible. For thermodynamics calculation, the temperature and pressure were assumed to be 470 °C and 1 atm, respectively. To mimic the typical HVPE process conditions, the partial pressures of O_2, GaCl, and $GaCl_3$ were set to 0.2, 2 × 10^{-7}, and 2 × 10^{-7} atm, respectively.

FEM simulation

The flow of injection gas in HVPE was calculated using the fluid dynamics module in COMSOL Multiphysics 5.5. The three-dimensional (3D) geometry model of the growth system was constructed based on the experimental observations and equipment drawing. To mimic a realistic vortex effect, the gas flow was described with a turbulence flow fluid. The motion of a gaseous fluid is calculated by solving the following Reynolds-averaged Navier–Stokes equations:

$$\rho(u\cdot\nabla)u = \nabla\cdot[-pI + (\mu + \mu_{\mathrm{T}})(\nabla u + (\nabla u)^T)] + F \quad (6)$$

$$\rho\nabla\cdot u = 0 \quad (7)$$

where ρ is density, u is the velocity field of a fluid, p is pressure, μ is viscosity, μ_{T} is turbulent viscosity, T indicates transpose, and F is the external forces applied to the fluid. The equations are solved using stationary boundary conditions with dense sampling of the background gas flow and displacement of the susceptor position. Referring to the experimental parameters, the boundary conditions of the inlet gas for O_2 and HCl were fixed to 300 sccm and 10 sccm, respectively. The 262 826 tetrahedral elements were generated to avoid numerical error and reduce computational resources due to the 3D structure of the simulation model.

The temperature distribution of gas flows induced by a heated chamber was simulated using the heat transfer module and linked with the fluid dynamics module. The temperature distribution of gas flows is calculated by solving the following equations:

$$\rho C_{\mathrm{p}}u\cdot\Delta T + \nabla\cdot q = Q \quad (8)$$

$$q = -k\nabla T \quad (9)$$

where C_{p} is the specific heat capacity at constant pressure, T is temperature, q is heat flux, Q is heat source, and k is thermal conductivity. To mimic the growth conditions, the boundary condition of the chamber was set to a fixed temperature of 470 °C, and the temperature of the inlet gas was set to room temperature, according to the experimental conditions.

Results and discussion

Theoretical study on the pre-reaction of the α-Ga_2O_3 growth by HVPE

To understand the pre-reaction of α-Ga_2O_3, we calculated the Gibbs free energy of the α-Ga_2O_3 formation from the two reactant gases, GaCl and $GaCl_3$, as shown in Fig. 2a. The formation of α-Ga_2O_3 considerably depends on the species of the reactant gas. The formation path from the $GaCl_3$ reactants can be either endothermic or exothermic depending on the process conditions, exhibiting a transition point at the partial pressure of O_2 ≈ 7 × 10^{-6} torr. In contrast, the formation of α-Ga_2O_3 from the GaCl reactant gas is always spontaneous and has large driving forces. This implies that α-Ga_2O_3 can be formed without the assistance of a substrate for the phase control;[30] thus, homogeneous nucleation can occur in the middle of the chamber. The homogeneous nucleation of Ga_2O_3 results in the formation of powders, and is the problematic pre-reaction, because the powders can attach to the chamber, tubes, and even substrates. When the powder is deposited on the substrates, it severely degrades the quality of the epitaxial growth.

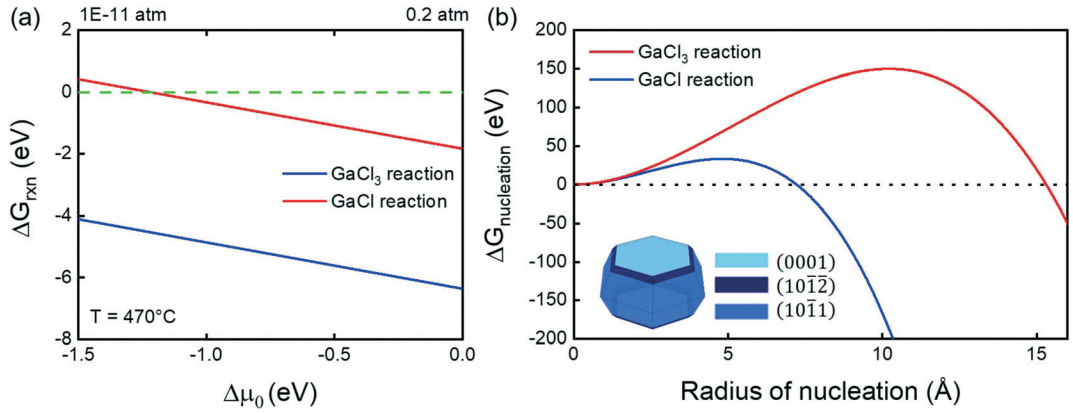

Fig. 2 Thermodynamics and energetics of the α-Ga_2O_3 growth using HVPE. (a) Calculated Gibbs reaction energy with respect to oxygen chemical potential. (b) Calculated Gibbs nucleation energy with respect to average surface energy obtained from the Wulff construction. The surface energy values were obtained from the literature.[29]

To understand the pre-reaction in further detail, we investigated the homogenous nucleation behavior. The shape of the particle formed from the homogeneous nucleation minimizes the surface energy[31] of the particle of fixed volume. Therefore, we carried out the Wulff construction from the surface energy of the representative orientation of the corundum structure α-Ga_2O_3. An α-Ga_2O_3 particle consists of (0001)-, (10–1–2)-, and (10–1–1)-oriented surfaces and is a 26-facet polyhedron. Because each facet is significantly large and the polyhedron is symmetric, the nucleation energetics of α-Ga_2O_3 can be calculated by considering those of a spherical surface, which is described as follows:

$$\Delta G_{\mathrm{nucle}}(r) = \frac{4}{3}\pi r^3 \Delta G_{\mathrm{v}} + 4\pi r^2 \sigma \qquad (10)$$

where r is the radius of nucleation, ΔG_{v} is the Gibbs free energy per volume of α-Ga_2O_3 obtained from the DFT calculations, and σ is the averaged surface energy.[29] As shown in Fig. 2b, the energy barrier for the nucleation from the GaCl reactant gas is very small, and almost corresponds to the formation of a single unit cell. In contrast, nucleation from the $GaCl_3$ reactant requires a large energy; therefore, homogenous nucleation is a rare event. The heterogeneous nucleation near the substrate easily forms α-Ga_2O_3 from the $GaCl_3$ reactant. This energetics shows that the pre-reaction is mainly due to the GaCl reactant gas. Therefore, the formation of GaCl gas should be suppressed, or it should be carefully controlled to avoid the pre-reaction.

Characterization

To clearly demonstrate the effect of suppressing the pre-reaction according to the inner tube carrier gas flow rate, the α-Ga_2O_3 epilayer surface was analyzed. Fig. 3a-1 and b-1

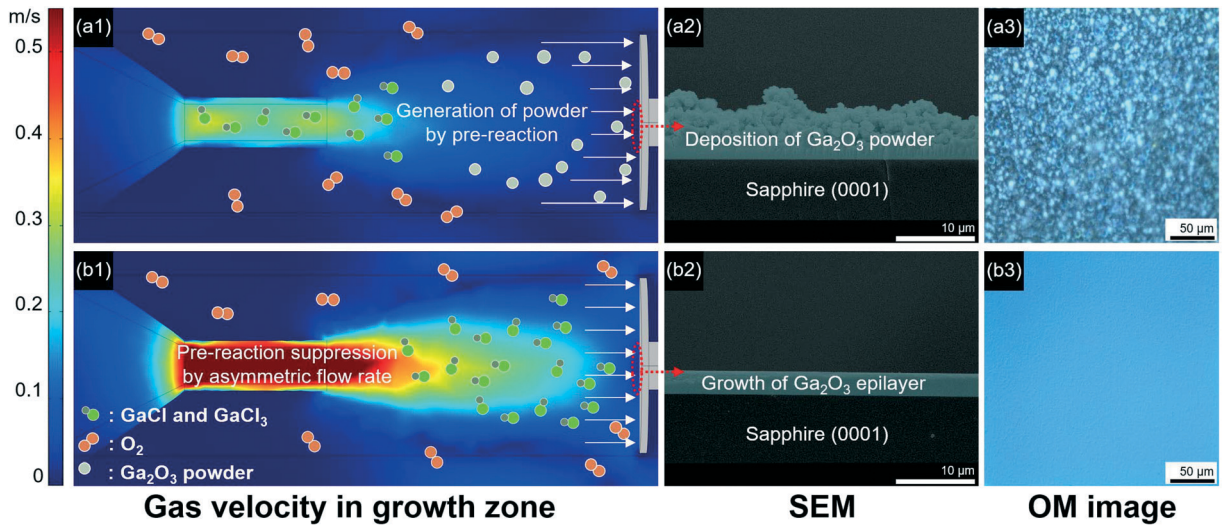

Fig. 3 (a-1) Gas velocity simulation in the growth zone with the inner tube carrier gas flow rate of 1100 sccm, and the corresponding (a-2) cross-view SEM and (a-3) surface OM images. (b-1) Gas velocity simulation in the growth zone with the inner tube carrier gas flow rate of 3900 sccm, and the corresponding (b-2) cross-view SEM and (b-3) surface OM images.

compare the gas velocity in the growth region through simulations. Fig. 3a-2–3 and b-2–3 show the α-Ga_2O_3 cross-view SEM and surface OM images with inner tube carrier gas flow rates of 1100 and 3900 sccm, respectively. As seen in the SEM (Fig. 3a-2) and OM (Fig. 3a-3) images, α-Ga_2O_3 did not grow properly as an epilayer, and it was observed that a huge amount of Ga_2O_3 powder was deposited on the substrate surface. This phenomenon occurred because the low inner tube carrier gas flow rate of 1100 sccm mainly increased the possibility of a pre-reaction between GaCl and O_2. As a result of the simulation shown in Fig. 3a-1, the velocity of the precursor and carrier gas coming out of the inner tube decreased rapidly; hence, the gas velocity was close to 0 m s^{-1} before reaching the substrate. This suggests that a pre-reaction can actively occur before the precursor gases reach the substrate, thereby increasing the possibility of homogeneous nucleation and powder formation. In contrast, when the carrier gas flow rate of the inner tube was 3900 sccm with the outer-shell gas flow rate of 600 sccm, a very clear and smooth surface morphology without powder was observed, as shown in Fig. 3b-2 and 3. This suggests that the pre-reaction can be sufficiently suppressed when the inner tube N_2 carrier gas flow rate is 3900 sccm. The simulation in Fig. 3b-1 indicates that increasing the N_2 gas flow rate to accelerate the overall gas velocity of the inner tube creates the conditions for GaCl and $GaCl_3$ to relatively quickly reach the substrate surface. Fig. S1† shows the photo, OM, and AFM images of the 2 inch α-Ga_2O_3 epilayer with different inner tube carrier gas flow rates of 1100, 3200, and 3900 sccm. The surface morphology is enhanced as the inner tube carrier gas flow rate is increased. In other words, the position of the pre-reaction in the growth region can be determined by adjusting the inner tube carrier gas flow rate. Experimental and simulation results show that the pre-reaction is effectively suppressed by the asymmetrical increase in the inner tube carrier gas flow rate.

Fig. 4 shows the resulting α-Ga_2O_3 epilayers grown on a 2 inch sapphire substrate with different susceptor positions, that is, at 5 cm and 10 cm. The susceptor position was determined by the distance between the inner tube edge and the substrate. The inner tube carrier gas flow rate was fixed at 3900 sccm. Although the pre-reaction was effectively suppressed by an asymmetrically increased inner tube carrier gas flow rate, it could result in significant differences in the distribution of the main precursors across the 2 inch substrate, affecting the quality and uniformity of the α-Ga_2O_3 epilayer. To uniformly grow high-quality α-Ga_2O_3 epilayers on a 2 inch substrate, it is necessary to solve the non-uniform dispersion of the precursors owing to the asymmetrically increased inner tube gas flow rate. To circumvent this problem, the susceptor position was adjusted from 5 cm to 11 cm (Fig. S2†). In Fig. S2,† the difference in the root mean square (RMS) surface roughness values based on the susceptor position is insignificant. Also, the RMS values within the 2 inch substrate were similar. This is because the N_2 carrier gas flow rate in the inner tube was 3900 sccm, which is sufficiently high to suppress the pre-reaction; consequently, Ga_2O_3 powder was not generated, and a smooth α-Ga_2O_3 epilayer was grown on the substrate. Fig. 4a-1 shows a real photo image of a 2 inch α-Ga_2O_3 epilayer, and Fig. 4a-2 and 3 show the results of flow velocity and temperature distribution simulations when the susceptor position is 5 cm. As seen in Fig. 4a-1, a ring-pattern groove appeared in the center of the 2 inch substrate. As mentioned above, this is one of the problems caused by the flow rate of the inner tube being asymmetrically very high compared to that of the outer-shell. According to the velocity simulation in Fig. 4a-2, a susceptor position of 5 cm induces a relatively large gas velocity difference of more than ~0.07 m s^{-1} between the substrate center and the periphery. Moreover, Fig. 4a-3 and S3† suggest that the combination of high gas velocity, significantly close susceptor position, and large

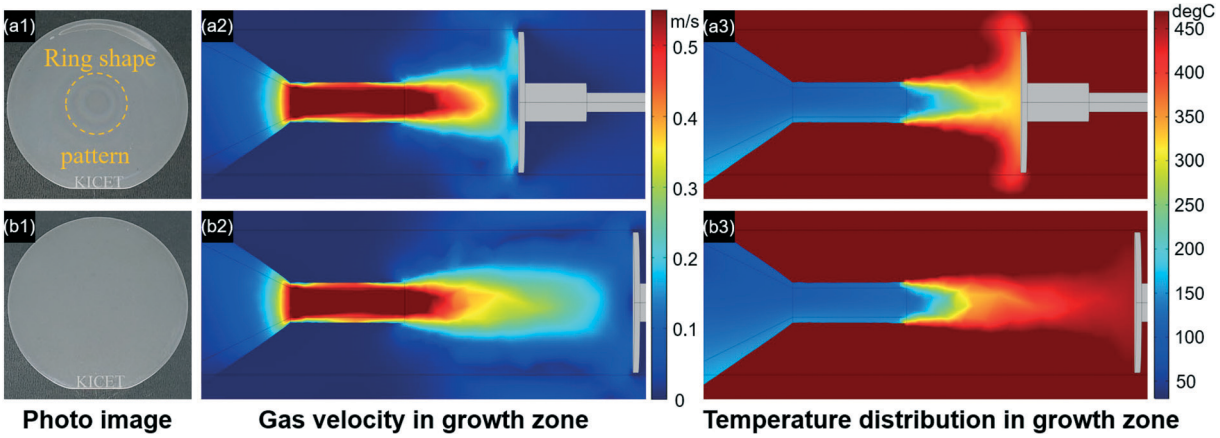

Fig. 4 (a-1) Photo image of an α-Ga_2O_3 epilayer grown on a 2 inch sapphire substrate with the inner tube carrier gas flow rate of 3900 sccm at a susceptor position of 5 cm, and the corresponding (a-2) gas velocity and (a-3) temperature simulations in the growth zone. (b-1) Photo image of an α-Ga_2O_3 epilayer grown on a 2 inch sapphire substrate with the inner tube carrier gas flow rate of 3900 sccm at a susceptor position of 10 cm, and the corresponding (b-2) gas velocity and (b-3) temperature simulations in the growth zone.

velocity deviation results in a larger difference in gas temperature compared to that in the set growth temperature. Interestingly, the gas temperature simulation on the substrate is approximated at 360 °C, which is more than 110 °C lower than the set growth temperature. The precursors reach the substrate before it is even heated to the set growth temperature and contribute to the growth of the epilayer. The low gas temperature of the substrate can lead to various defects and degradation of crystallinity in the α-Ga_2O_3 epilayer during the growth.[21,32,33] However, most of these problems are resolved when the susceptor position is increased to 10 cm. As shown in Fig. 4b-1, a clean α-Ga_2O_3 epilayer was grown without any groove pattern on the surface. Fig. 4b-2 shows that the gas velocity deviation across the 2 inch substrate is less than ~0.02 m s^{-1}. According to the simulation models in Fig. 4b-3 and S3,† when the susceptor position is more than 10 cm, the gas temperature on the substrate can be uniformly distributed and the substrate has sufficient time to reach the set growth temperature.

An F20-UV was used to investigate the effect of the correlation between the susceptor position and the gas velocity on the thickness uniformity of the α-Ga_2O_3 epilayer grown on a 2 inch substrate. Fig. 5 shows the thickness uniformity of the α-Ga_2O_3 epilayers grown on 2 inch substrates with different susceptor positions, that is, from 5 cm to 11 cm. The thickness of the α-Ga_2O_3 epilayers at the center of the substrate varies from approximately 300 nm to 1100 nm without significant deviation depending on the susceptor position, as shown in Fig. 5. Furthermore, the thickness of the α-Ga_2O_3 epilayers at the side of the substrate exhibits deviations of ±200 nm or more and ±50 nm or less before and after the susceptor position is 10 cm, respectively. The susceptor position of 5 cm provided a thin center thickness due to significantly fast gas velocity and the largest thickness deviation of approximately 41% due to the predicted large gas velocity difference across the 2 inch substrate. In contrast, when the susceptor position is 10 cm, the thickness deviation for the entire 2 inch substrate is approximately 2.6%. Fig. 5b shows the highest growth rate when the susceptor position is 10 cm, and the thickness of the α-Ga_2O_3 epilayer tends to decrease as the susceptor position approaches or moves away from the inner tube. The highest growth rate of 110 nm min^{-1} was achieved within the 2 inch substrate at the susceptor position of 10 cm. As expected from the gas velocity simulation at the susceptor position of 10 cm, the gas velocity on the substrate is approximately ~0.05 m s^{-1}, and the deviation in the gas velocity is 2.4% (Fig. S3†). It is considered that when the susceptor position is 11 cm, the growth rate is reduced because the amount of gas reaching the substrate is reduced due to the decreased gas velocity. As a result, when the susceptor position is 10 cm, a uniform gas velocity on the substrate is expected from the results of gas velocity simulation (Fig. S3†), and the highest growth rate and approximately 97.4% thickness uniformity of the α-Ga_2O_3 epilayer were obtained.

The crystal structure of the epilayer was investigated by HR-XRD. Fig. 6a shows the HR-XRD 2θ scan spectra of the α-Ga_2O_3 epilayers with different susceptor positions. Only two sharp diffraction peaks corresponding to the (0006) plane of α-Ga_2O_3 and Al_2O_3 were observed. When the susceptor position is 10 cm or more, the α-Ga_2O_3 (0006) peak appears at 40.26° (JCPDS no.06-0503); however, as the susceptor position becomes closer to the inner tube, the peak tends to shift to 40.18°. This change in the peak position suggests that the compressive residual stress in the α-Ga_2O_3 epilayer increases as the susceptor position approaches the inner tube. Fig. 6b shows the full width at half maximum (FWHM) values of the HR-XRD rocking curve of the (0006) and (10–14) reflections to evaluate the crystal quality of the α-Ga_2O_3 epilayers (Fig. S5†). At the susceptor position of 10 cm, the FWHM values of (0006) and (10–14) of the α-Ga_2O_3 epilayer were the minimum at 29 and 1301 arcsec, respectively. These FWHM values were equivalent to those of high-quality α-Ga_2O_3 epilayers grown with HVPE.[7,21,37] The crystal quality

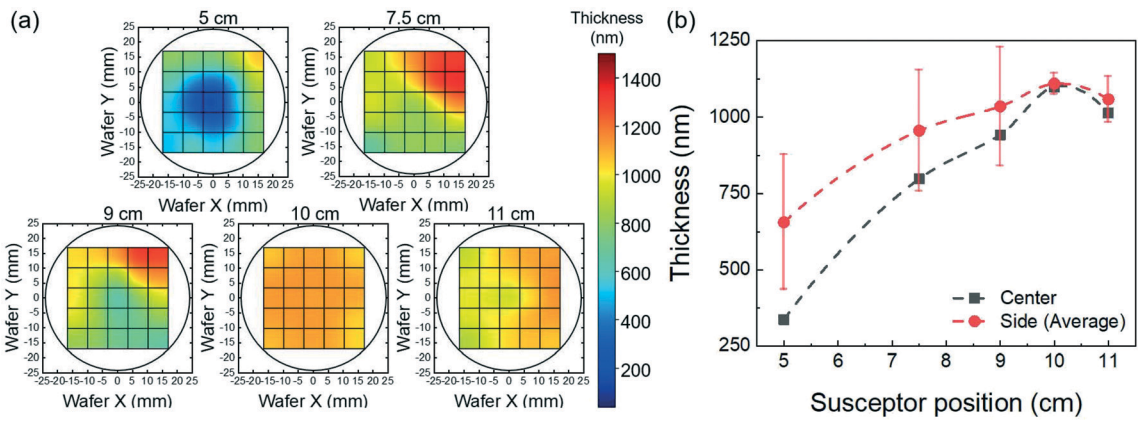

Fig. 5 (a) Thickness uniformity of α-Ga_2O_3 epilayers grown on 2 inch sapphire substrates with different susceptor positions (5–11 cm). (b) Relationship between the thickness of an α-Ga_2O_3 epilayer, at the center and side of a 2 inch sapphire substrate, and the susceptor position.

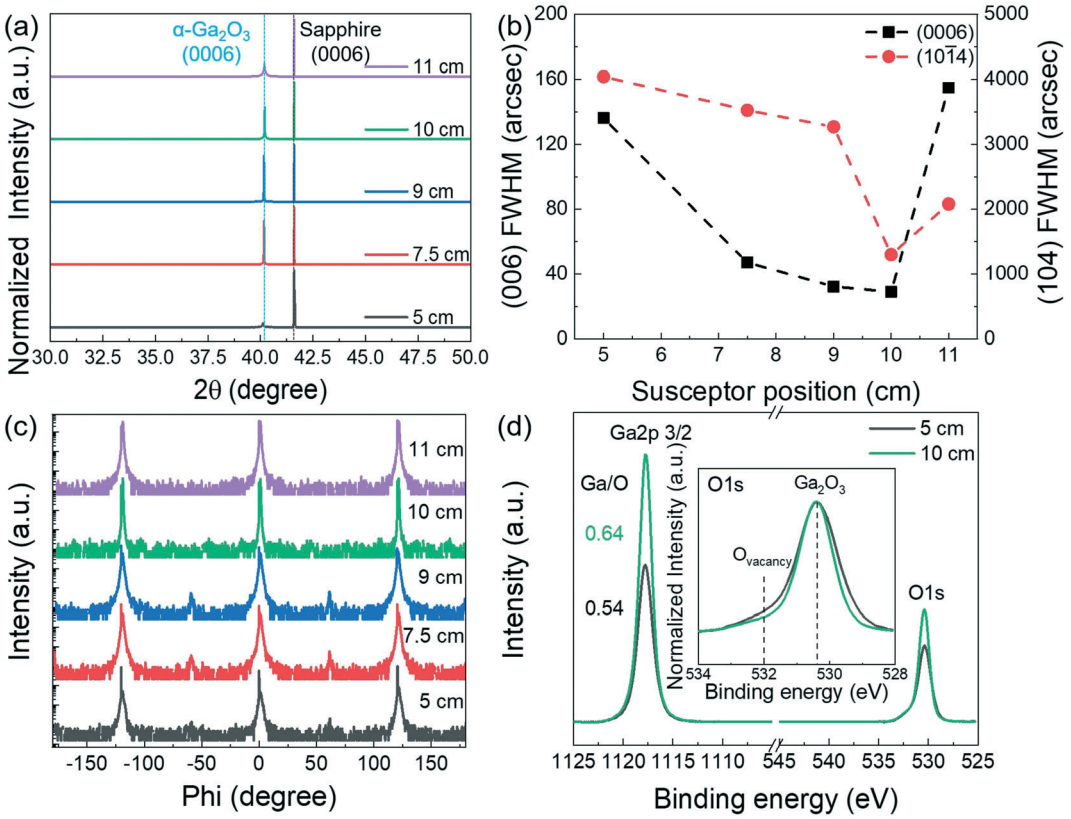

Fig. 6 (a) HR-XRD 2θ scan spectra, (b) FWHM values of the HR-XRD rocking curve of the (0006) and (10–14) reflections, and (c) HR-XRD phi-scan of the (10–14) reflection of the α-Ga_2O_3 epilayers grown at different susceptor positions. (d) XPS Ga2p 3/2 and O1s peak data of the α-Ga_2O_3 epilayers grown at the susceptor positions of 5 cm and 10 cm.

of the grown α-Ga_2O_3 epilayers improved as the susceptor position approached 10 cm. In the HR-XRD phi-scan (Fig. 6c), three dominant peaks were observed at 120 degree intervals, and three additional small peaks were identified when the susceptor position was closer than 9 cm to the inner tube. The three small peaks indicated the degradation of the α-Ga_2O_3 epilayer quality. The reason for the degradation of the α-Ga_2O_3 epilayer quality is that the predicted temperature attained by the substrate in the simulation is lower than the set growth temperature (Fig. S4†). This may be a result of the dual positioning domains formed during the initial nucleation and lateral coalescence stages below the susceptor position of 9 cm.[34] In Fig. 6d, the average Ga/O ratio of the α-Ga_2O_3 epilayers was estimated from the integrated peak area ratio of the deconvoluted XPS component calibrated using the sensitivity factor.[35–37] The Ga/O ratios were calculated to be 0.52 and 0.64 with the susceptor positions at 5 cm and 10 cm, respectively. The Ga/O ratio at the susceptor position of 10 cm is similar to 0.67 for stoichiometric bulk Ga_2O_3. Thus, it is considered that oxygen-related and oxygen vacancies decrease as the susceptor position approaches 10 cm. In addition, the two O1s peaks located at 530.4 eV and 532.0 eV represent the Ga–O bond and the oxygen or oxygen-related vacancies, respectively.[37,38] The oxygen vacancy region is larger at 5 cm than 10 cm due to the low temperature and high gas velocity predicted in the simulation. This indicates that defects exist in the α-Ga_2O_3 epilayer grown at the susceptor position of 5 cm, which is consistent with the HR-XRD results.

Conclusions

In summary, we used the HVPE method to optimize the growth conditions for high-quality and uniform α-Ga_2O_3 epilayers on a 2 inch sapphire substrate. The asymmetric N_2 carrier gas flow rate between the inner tube and outer-shell effectively suppressed the pre-reaction of the main precursors. The non-uniform distribution of the main precursors on the substrate caused by the asymmetric N_2 carrier gas flow rate was compensated by controlling the distance between the susceptor and the inner tube. Gas velocity and temperature simulations were performed to analyze the correlation between the growth results of the α-Ga_2O_3 epilayers and the experimental variables. As a result, the complementary relationships between the inner tube flow rate and pre-reaction and the susceptor position and growth uniformity were well presented.

The sample grown under optimal conditions by controlling two main variables showed 97.4% thickness uniformity on a 2 inch substrate. In the HR-XRD measurements, the FWHM values of the (0006) and (10–14) rocking curves were obtained as 29.16 arcsec and 1301.54

arcsec, respectively. Furthermore, the presence of only three peaks in the (10–14) phi-scan indicates a high-quality crystalline epilayer without twinning. The Ga/O ratio in the XPS data was 0.64, which is similar to the ideal value. Experimental and simulation studies on the complementary relationship between the carrier gas flow rate and susceptor position provided a high-quality and uniform 2 inch α-Ga_2O_3 epilayer, which would lead to the realization of large-area growth of α-Ga_2O_3 epilayers over 4 inches.

Conflicts of interest

The authors declare no competing financial interest.

Acknowledgements

This work was supported by the Ceramic Strategic Research Program (KPP19003-3 and KPP20004-2) through the Korea Institute of Ceramic Engineering & Technology (KICET). We gratefully acknowledge support from the National Research Foundation of Korea (NRF-2019R1F1A1058554 and 2020M3H4A3081796).

References

1 S. J. Pearton, J. Yang, P. H. Cary IV, F. Ren, J. Kim, M. J. Tadjer and M. A. Mastro, *Appl. Phys. Rev.*, 2018, **5**, 011301.
2 M. A. Mastro, A. Kuramata, J. Calkins, J. Kim, F. Ren and S. J. Pearton, *ECS J. Solid State Sci. Technol.*, 2017, **6**, 356–359.
3 S. I. Stepanov, V. I. Nikolaev, V. E. Bougrov and A. E. Romanov, *Rev. Adv. Mater. Sci.*, 2016, **44**, 63–86.
4 R. Roy, V. G. Hill and E. F. Osborn, *J. Am. Chem. Soc.*, 1952, **74**, 719–722.
5 J. Furthmüller and F. Bechstedt, *Phys. Rev. B*, 2016, **93**, 115204.
6 M. Oda, R. Tokuda, H. Kambara, T. Tanikawa, T. Sasaki and T. Hitora, *Appl. Phys. Express*, 2016, **9**, 021101.
7 D. W. Jeon, H. Son, J. Hwang, A. Y. Polyakov, N. B. Smirnov, I. V. Shchemerov, A. V. Chernykh, A. I. Kochkova, S. J. Pearton and I. H. Lee, *APL Mater.*, 2018, **6**, 121110.
8 Q. He, W. Mu, H. Dong, S. Long, Z. Jia, H. Lv, Q. Liu, M. Tang, X. Tao and M. Liu, *Appl. Phys. Lett.*, 2017, **110**, 093503.
9 J. Yang, F. Ren, M. Tadjer, S. J. Pearton and A. Kuramata, *ECS J. Solid State Sci. Technol.*, 2018, **7**, 92–96.
10 Y. Yao, L. A. M. Lyle, J. A. Rokholt, S. Okur, G. S. Tompa, T. Salagaj, N. Sbrockey, R. F. Davis and L. M. Porter, *ECS Trans.*, 2017, **80**, 191–196.
11 R. Cariou, W. Chen, J. L. Maurice, J. Yu, G. Patriarche, O. Mauguin, L. Largeau, J. Decobert and P. R. i Cabarrocas, *Sci. Rep.*, 2016, **6**, 1–8.
12 H. W. Kim, H. Ko, Y. C. Chung and S. B. Cho, *J. Eur. Ceram. Soc.*, 2021, **41**, 611–616.
13 E. Ahmadi and Y. Oshima, *J. Appl. Phys.*, 2019, **126**, 160901.
14 Z. Chenga, M. Hanke, P. Vogt, O. Bierwagen and A. Trampert, *Appl. Phys. Lett.*, 2017, **111**, 162104.
15 D. Shinohara and S. Fujita, *Jpn. J. Appl. Phys.*, 2008, **47**, 7311–7313.
16 Y. Oshima, E. G. Víllora and K. Shimamura, *Appl. Phys. Express*, 2015, **8**, 055501.
17 J. Wu, L. Zhao, D. Wen, K. Xu, Z. Yang, G. Zhang, H. Li and R. Zuo, *Appl. Surf. Sci.*, 2009, **255**, 5926–5931.
18 L. Zhao, J. Wu, K. Xu, Z. Yang and G. Zhang, *Appl. Surf. Sci.*, 2009, **255**, 8003–8009.
19 Y. Shao, Y. Dai, X. Hao, Y. Wu, L. Zhang, H. Zhang and Y. Tian, *CrystEngComm*, 2013, **15**, 7965–7969.
20 Y. Oshima, K. Kawara, T. Oshima, M. Okigawa and T. Shinohe, *Semicond. Sci. Technol.*, 2020, **35**, 055022.
21 H. Son and D. W. Jeon, *J. Alloys Compd.*, 2019, **773**, 631–635.
22 S. A. Safvi, N. R. Perkins, M. N. Horton, R. Matyi and T. F. Kuech, *J. Cryst. Growth*, 1997, **182**, 233–240.
23 C. E. C. Dam, A. P. Grzegorczyk, P. R. Hageman, R. Dorsman, C. R. Kleijn and P. K. Larsen, *J. Cryst. Growth*, 2004, **271**, 192–199.
24 E. Richter, Ch. Hennig, M. Weyers, F. Habel, J. D. Tsay, W. Y. Liu, P. Brückner, F. Scholz, Y. Makarov, A. Segal and J. Kaeppeler, *J. Cryst. Growth*, 2005, **277**, 6–12.
25 Y. Yao, S. Okur, L. A. M. Lyle, G. S. Tompa, T. Salagaj, N. Sbrockey, R. F. Davis and L. M. Porter, *Mater. Res. Lett.*, 2018, **6**, 268–275.
26 G. Kresse and J. Furthmüller, *Phys. Rev. B: Condens. Matter Mater. Phys.*, 1996, **54**, 11169–11186.
27 J. P. Perdew, K. Burke and M. Ernzerhof, *Phys. Rev. Lett.*, 1996, **77**, 3865–3868.
28 H. J. Monkhorst and J. D. Pack, *Phys. Rev. B: Solid State*, 1976, **13**, 5188–5192.
29 W. Sun and G. Ceder, *Surf. Sci.*, 2018, **669**, 50–56.
30 S. B. Cho and R. Mishra, *Appl. Phys. Lett.*, 2018, **112**, 162101.
31 J. M. Rahm and P. Erhart, *J. Open Source Softw.*, 2020, **5**, 1944.
32 Y. Zhuo, Z. Chen, W. Tu, X. Ma, Y. Pei and G. Wang, *Appl. Surf. Sci.*, 2017, **420**, 802–807.
33 H. Ghadi, J. F. McGlone, Z. Feng, A. F. M. A. U. Bhuiyan, H. Zhao, A. R. Arehart and S. A. Ringel, *Appl. Phys. Lett.*, 2020, **117**, 172106.
34 T. C. Ma, X. H. Chen, Y. Kuang, L. Li, J. Li, F. Kremer, F. F. Ren, S. L. Gu, R. Zhang, Y. D. Zheng, H. H. Tan, C. Jagadish and J. D. Ye, *Appl. Phys. Lett.*, 2019, **115**, 182101.
35 R. O'Donoghue, J. Rechmann, M. Aghaee, D. Rogalla, H. W. Becker, M. Creatore, A. D. Wieck and A. Devi, *Dalton Trans.*, 2017, **46**, 16551–16561.
36 P. Song, Z. Wu, X. Shen, J. Kang, Z. Fang and T. Y. Zhang, *CrystEngComm*, 2017, **19**, 625–631.
37 H. Son, Y. J. Choi, J. Hwang and D. W. Jeon, *ECS J. Solid State Sci. Technol.*, 2019, **8**, 3024–3027.
38 S. Kim, H. Ryou, I. G. Lee, M. Shin, B. J. Cho and W. S. Hwang, *RSC Adv.*, 2021, **11**, 7338–7346.

